HHS Public Access

Author manuscript

Nat Chem Biol. Author manuscript; available in PMC 2011 June 01.

Published in final edited form as:

Nat Chem Biol. 2010 December ; 6(12): 900–906. doi:10.1038/nchembio.467.

Inhibitors of protein disulfide isomerase suppress apoptosis induced by misfolded proteins

Benjamin G. Hoffstrom[1], **Anna Kaplan**[1], **Reka Letso**[1], **Ralf Schmid**[3], **Gregory J. Turmel**[3], **Donald C. Lo**[3], and **Brent R. Stockwell**[1,2,*]

[1] Howard Hughes Medical Institute, Department of Biological Sciences, Columbia University, 614 Fairchild Center, 1212 Amsterdam Avenue, New York, New York 10027, USA

[2] Department of Chemistry, Columbia University, 614 Fairchild Center, 1212 Amsterdam Avenue, New York, New York 10027, USA

[3] Center for Drug Discovery and Department of Neurobiology, Duke University Medical Center, 4321 Medical Park Drive, Suite 200, Durham, North Carolina 27704, USA

Abstract

A hallmark of many neurodegenerative diseases is accumulation of misfolded proteins within neurons, leading to cellular dysfunction and cell death. Although several mechanisms have been proposed to link protein misfolding to cellular toxicity, the connection remains enigmatic. Here, we report a cell death pathway involving protein disulfide isomerase (PDI), a protein chaperone that catalyzes isomerization, reduction, and oxidation of disulfides. Through a small-molecule-screening approach, we discovered five structurally distinct compounds that prevent apoptosis induced by mutant huntingtin protein. Using modified Huisgen cycloaddition chemistry, we then identified PDI as the molecular target of these small molecules. Expression of polyglutamine-expanded huntingtin exon 1 in PC12 cells caused PDI to accumulate at mitochondrial-associated-ER-membranes and trigger apoptotic cell death, via mitochondrial outer membrane permeabilization. Inhibiting PDI in rat brain cells suppressed the toxicity of mutant huntingtin exon1 and Aβ peptides processed from the amyloid precursor protein. This pro-apoptotic function of PDI provides a new mechanism linking protein misfolding and apoptotic cell death.

INTRODUCTION

Protein folding diseases encompass a large class of neurological disorders, including Alzheimer's disease (AD), Parkinson's disease (PD), amyotrophic lateral sclerosis (ALS), Huntington disease (HD), and prion diseases[1]. Huntington disease, for example, is a

*To whom correspondence should be addressed. bstockwell@columbia.edu.

AUTHOR CONTRIBUTIONS

B.G.H. and B.R.S designed the experiments. B.G.H. performed the experiments and analyzed the data with B.R.S. A.K. assisted with the library screening, characterization of hit compounds, analysis of synthesized analogs, validation studies, and structural identification of securinine. R.L. performed the PDI and Bcl-2 overexpression experiments. R.S., G.J.T., and D.C.L. provided the cortical-striatal brain slice data. B.G.H. and B.R.S. wrote the manuscript.

The authors declare no competing financial interests.

polyglutamine disease caused by a mutation that expands a CAG repeat region within the *huntingtin* gene. This mutation leads to a polyglutamine-expanded huntingtin protein that improperly folds; ultimately, this causes cell death in the striatum and cortex[2]. Precisely how mutant huntingtin causes HD remains unclear; however, both humans and animal models of HD show markers of apoptotic cell death[3–9].

Apoptosis is an elaborate cell death program essential for neuronal pruning during development, and for the clearance of cells that become dysfunctional[10]. The most common form of apoptosis proceeds via the intrinsic pathway through mitochondria. In this pathway, an initiation event triggers mitochondrial outer membrane permeabilization (MOMP), which is a perforation in the outer mitochondrial membrane created by oligomerized Bax or Bak protein[11,12]. The induction of MOMP leads to the release of proteins (e.g., cytochrome c and Smac) from the mitochondrial intermembrane space, which in turn activates caspase enzymes that degrade key structural and functional components of the cell[13]. Several upstream triggers of MOMP have been reported, including DNA damage, loss of cell adhesion, growth factor withdrawal, and endoplasmic reticulum (ER) stress[14]. The endoplasmic reticulum is an important site of protein folding, dysregulation of which can activate a cell death cascade. However, in some neurodegenerative diseases (e.g., HD and PD) the aberrant protein accumulates in the cytosol, suggesting additional mechanisms exist to monitor protein folding and to control cellular homeostasis.

We used a cell-based model of HD to screen tens of thousands of synthetic compounds and natural products for their ability to suppress cell death induced by polyglutamine-expanded huntingtin exon one. We then used Huisgen cycloaddition chemistry (or “Click-Chemistry”) to identify protein disulfide isomerase (PDI) as the molecular target of multiple active compounds. We found that in response to expression of mutant huntingtin exon one, PDI becomes concentrated at ER-mitochondrial junctions and induces MOMP. The death-suppressing compounds we identified in our screen block this cascade by inhibiting the enzymatic activity of PDI. Finally, we show that inhibiting PDI activity in normal rat brain cells suppresses the toxicity of misfolded huntingtin and APP/Aβ protein.

RESULTS

Small molecule inhibitors of apoptosis

To identify small molecule suppressors of polyglutamine-induced apoptosis, we adapted a PC12 cell model of HD into a high-throughput screening format[15]. In this system, PC12 cells were transfected with the first exon of the human *huntingtin* (htt) gene, containing either wild-type (Q25) or mutant (Q103) polyglutamine (polyQ) repeats, fused to EGFP; we refer to these two cell lines as “Q25” and “Q103”. Protein expression was induced by tebufenozide, an ecdysone analog that binds to the *Bombyx mori* ecdysone receptor. Following addition of tebufenozide to the culture medium, mutant cells accumulated peri-nuclear inclusion bodies (~12 hours) and underwent apoptosis (15–48 hours), which we quantified using Alamar Blue, a fluorescent indicator of cell viability (Fig. 1).

We screened 68,887 compounds derived from small molecule libraries containing natural products, natural product analogs, synthetic drug-like compounds, and annotated,

biologically active compounds (Fig. 1d). Hit compounds from the primary screen were prioritized based on their potency in a dose-response curve. These hits were filtered to eliminate those that were likely acting through non-polyQ-dependent mechanisms (e.g., compounds that suppress htt protein expression, or compounds that act as general caspase inhibitors; Supplementary Fig. 1 and data not shown). The top five hits were prioritized based on both potency and efficacy of cell viability rescue and the compounds' capacity to restore "normal" (uninduced) cell morphology to induced Q103-expressing cells (Fig. 2 and Supplementary Fig. 2). Interestingly, these compounds did not significantly alter the accumulation of htt-Q103 inclusion bodies (Supplementary Fig. 3).

Identifying small molecule targets

A covalent interaction between a small molecule and its target protein can increase the facility of target identification. Considering that alpha-chloromethylketone-like moieties are frequently used for irreversibly inhibiting proteases, we speculated that compound 16F16, with its related chloroacetyl moiety, was covalently binding its target protein. In support of this hypothesis, we found that an analog of 16F16 lacking the chloro substituent was inactive. Additional structure-activity studies of 16F16 revealed that changing the ester from methyl to ethyl did not affect its activity. However, modifications at this site that incorporated biotin or fluorescein affinity tags resulted in a complete loss of activity (data not shown). Therefore, we identified a site on 16F16 that could tolerate small structural changes; however, incorporation of traditional large affinity handles was not compatible with activity(see Supplementary Methods).

To overcome this problem, we adapted the copper-mediated Huisgen 1,3,-dipolar cycloaddition of an azide to an alkyne; this reaction has been shown to be bio-orthogonal and facile in the presence of cell lysates[16–20]. The advantage in using this approach was that we could introduce a minimal structural modification to 16F16 (e.g., a terminal propargyl alkyne) without losing biological activity. Once the alkyne-derivatized-16F16 was covalently bound to its target protein, we could subsequently attach a tag (e.g., fluorescein-azide or rhodamine-azide) via modified Huisgen cycloaddition reaction (Fig. 3a).

Following synthesis, we tested the alkyne analog of 16F16 (16F16A) for its ability to suppress Q103-induced apoptosis and found that the alkyne modification did not disrupt target binding. We then coupled azidofluorescein to PC12-Q103 lysates treated with 16F16A, and purified the resulting fluorescein-tagged proteins with an anti-fluorescein antibody. By mass spectrometry we identified two isoforms of protein disulfide isomerase (PDIA1 and PDIA3) as specific targets of 16F16A which we then confirmed by competitive binding assays, labelling purified PDI, and a Western blot of affinity purified target proteins (Fig. 3b–d, Supplementary Tables 1, 2, and 3).

In performing the competitive binding assays, we discovered that in addition to 16F16, the other four active hits from the screen (Fig. 2) also showed competitive inhibition of 16F16A binding to PDI, whereas inactive analogs did not (Fig. 3c). Given the ability of PDI to function as a disulfide reductase, we tested whether cystamine, a simple organic disulfide that has been shown to delay onset of neuropathological sequellae in animal models of HD and PD, could compete for 16F16A binding to PDI[21–24]. Cystamine was able to compete

with 16F16A for binding to PDI, whereas hypotaurine, an inactive cystamine analog, did not have this effect (Fig. 3c). Given the results of the PDI binding experiments, we went on to test these hit compounds, along with cystamine, for their ability to inhibit the enzymatic activity of PDI *in vitro*. Here, we observed a striking correlation between the PDI binding assays (Fig. 3c), inhibition of PDI enzymatic activity, and rescue of polyQ-induced cell death (Fig. 4).

PDI within mitochondrial-associated-membranes induces MOMP

In humans, protein disulfide isomerases (EC 5.3.4.1) constitute a family of at least 17 enzymes of the thioredoxin superfamily that function primarily in the ER as chaperone proteins and facilitate disulfide bond rearrangements via catalysis of thiol-disulfide-exchange[25,26]. In addition to their well-described function in the ER, PDI proteins have been reported in the cytosol and on mitochondria, where their physiological functions are less clear[25,27,28]. We examined the localization of PDI over time in subcellular fractions of induced Q25 and Q103 cells and found that following induction, Q103 cells differentially accumulated PDI in the mitochondrial fraction (2.8 fold over Q25 at 24 hours; Fig. 5a–c). Inhibiting PDI activity with 16F16 further increased mitochondrial accumulation of PDI in Q103 cells (5.3 fold over Q25 at 24 hours). The latter result suggested that by inhibiting the enzymatic activity of PDI, we were allowing levels of the mitochondrial-associated PDI to increase beyond a point that would otherwise induce apoptosis. To identify more precisely the localization of mitochondrial-associated PDI we performed protease-shaving analysis of the ER/microsomal and crude (sucrose gradient purified) mitochondrial fractions. These experiments showed that the mitochondrial-associated PDI was similar to the ER/microsomal PDI in that it was protected from trypsin digestion (Supplementary Fig. 4). Mitochondria are known to contact the ER through mitochondrial-associated-membranes (MAM; Fig. 5d)[29]. This membrane fraction, which is an extension of the endoplasmic reticulum (ER) that contacts mitochondria, has been shown to function as an important regulatory connection between the ER and mitochondria[30–32]. When we purified MAMs from PC12 mitochondria via Percoll gradient sedimentation, we found that the mitochondrial-associated PDI was predominantly localized to the MAM compartment (Fig. 5e).

Inhibiting PDI in Q103-expressing cells suppresses mitochondrial release of cytochrome c and subsequent activation of caspases (Fig. 5f and Supplementary Fig. 1). In light of finding increased levels of PDI in association with mitochondria isolated from Q103-expressing cells, we hypothesized that PDI may engage MOMP by interacting with proapoptotic proteins associated with the outer mitochondrial membrane at a critical concentration ratio. We tested this hypothesis *in vitro* using a “MOMP assay”, whereby we added purified PDI to isolated mitochondria and monitored the mitochondrial release of cytochrome c. Here, we found that under physiological conditions, there is a threshold concentration of PDI that can induce MOMP and that small molecule PDI-inhibitors suppressed this activity (Fig. 5g). Finally, overexpressing PDIA1 or PDIA3 in PC12 cells simulated the MOMP assay in a cellular context and induced apoptosis that could be rescued by blocking the catalytic activity of PDI with small molecule inhibitors (Fig. 5h–i).

To further characterize and validate the mechanism of PDI-induced apoptosis, we evaluated the PDI-induced MOMP mechanism in two additional model systems. The induction of MOMP is primarily mediated by the formation of homo-oligomeric channels of Bax or Bak in the mitochondrial outer membrane[12]. Therefore, we tested whether PDI could induce MOMP in mitochondria isolated from wild type or Bax/Bak double-knockout MEF cells[33]. These experiments showed that PDI could induce MOMP in wild-type MEF mitochondria, but mitochondria from Bax/Bak double-knockout cells were resistant (Fig. 6a). The mechanism governing the assembly of Bax/Bak homo-oligomeric complexes is not well understood; however, it has been shown that Bax can form an active oligomeric complex via oxidation of conserved cysteine residues[34]. We investigated the possibility that PDI could induce MOMP by oxidizing Bax or Bak and found that wild-type MEF mitochondria undergoing MOMP had disulfide-linked oligomers of Bak, but not Bax (Fig. 6a and Supplementary Fig. 7). However, the combined knockdown of Bak and Bax protein in PC12-Q103 cells showed an additive rescue of apoptosis suggesting that both Bax and Bak function as downstream cell death effectors (Supplementary Fig. 5). In addition, overexpressing Bcl-2 protein in PC12-Q103 cells also suppressed apoptosis, suggesting that Bcl-2 can antagonize PDI-induced activation of Bax and Bak (Supplementary Fig. 5).

We next tested the protective effects of PDI inhibitors in a corticostriatal brain slice model for mutant htt-exon 1 (htt-N90Q73)-induced neurotoxicity[35–37]. Of three PDI inhibitors tested, all showed dose-dependent rescue of htt-N90Q73-induced neurotoxicity in medium spiny neurons (MSNs) in the striatal region of these brain slices (Fig. 6b–e). We also confirmed the mechanism of PDI-induced toxicity in MSNs by rescuing htt-N90Q73 neurotoxicity with PDIA3 shRNA (Fig. 6f and Supplementary Fig. 6).

To broaden the scope of our study, we repeated these experiments in rat brain slices expressing amyloid precursor protein (APP), which is processed in situ to Aβ peptides, the causative agents central to the amyloid cascade hypothesis of Alzheimer's disease[38,39]. Similar to the results obtained for mutant huntingtin, we observed a dose-dependent rescue of Aβ toxicity in pyramidal neurons when PDI was inhibited by small molecules or shRNA knockdown (Fig. 6g–j).

DISCUSSION

Suppressing caspase activation or blocking the release of caspase cleavage products has been shown to be effective in delaying disease progression in transgenic mouse models of ALS, HD, and AD[40–45]. In our screen for suppressors of polyQ-induced cell death, we identified several compounds that act upstream of caspase activation by targeting the A1 and A3 isoforms of PDI. As chaperone proteins, PDIs are involved in the recognition and repair of aberrant protein assembly and show increased expression in patients with ALS, PD, and Creutzfeldt-Jakob disease (human prion disease)[46–48]. The initial upregulation of PDIs constitutes a defense mechanism to repair misfolded proteins and restore normal cellular homeostasis[49]. However, as we have shown here in brain slice assays for mutant htt-N90Q73 or APP/Abeta-induced neurodegeneration, ultimately limiting increases in PDI activity and/or expression with small molecule compounds or shRNA, respectively, provides net neuroprotective benefit. Thus, analogous to expression of p53, which accumulates to

repair damaged DNA, but induces apoptosis at extreme levels of DNA damage, PDI is also capable of engaging a cell death cascade when it accumulates at high levels in response to misfolded proteins.

The PDI apoptosis pathway appears to be specific for misfolded proteins, since other apoptotic stimuli (e.g., chemical inducers and serum withdraw) are not suppressed by inhibiting PDI (Supplementary Fig. 9). Furthermore, the ability of PDI to induce MOMP in isolated mitochondria and its inhibition-mediated rescue of apoptosis in cells depleted of BiP/GRP78, a key regulator of the unfolded protein response, suggests that the PDI pathway operates independently of factors that regulate ER stress-induced apoptosis (Supplementary Fig. 10). From our analysis of PDI-induced MOMP in isolated mitochondria, PDI can oligomerize Bak in the outer mitochondrial membrane by inter-molecular oxidation of Bak cysteine residues. Although we have not excluded the involvement of Bak/Bax-activating intermediates, structural properties and conserved PDIA1/A3 residues required for oxidative activity may explain why A1 and A3 were the two PDI isoforms identified in our screen[26].

Complete inhibition of PDI catalytic activity, as observed with high concentrations of inhibitors and knockdown with shRNA, is toxic in cultured cell lines such as PC12. Despite the narrow therapeutic index observed in PC12 cells, our experiments using rat brain slice explants demonstrate protective efficacy against polyglutamine and APP/Aβ toxicity in neurons. *In vivo*, cystamine has been shown in several studies to extend survival and to improve motor performance in HD and PD animal models; however, its mechanism of action has remained unclear[21–24,50]. In our study, we show that cystamine competitively binds to PDI and inhibits its enzymatic activity *in vitro*. In cells, cystamine suppresses intrinsic apoptosis induced by polyQ-expanded huntingtin and partially blocks PDI-induced MOMP in purified mitochondria. These results suggest that the protective effect of cystamine in HD and PD model mice may be through inhibition of PDI.

In summary, we used a novel strategy to identify PDI as a target of several compounds that suppress polyglutamine-induced and APP/Aβ-induced neuronal degeneration. Furthermore, we have identified a cell death pathway regulated by PDI, a chaperone protein important for quality control in protein folding. A comprehensive understanding of how the PDI cell death pathway is controlled may aid in discovering therapeutics to treat protein misfolding diseases.

METHODS

Cell culture and transfection

We used a PC12 model of HD for screening[15]. Briefly, PC12 cells transfected with pBWN, an ecdysone-responsive expression vector containing DNA inserts encoding exon-1 of human *huntingtin* (including proline-rich segment and either 25 or 103 mixed CAG/CAA repeats, EGFP, and neomycin resistance gene) were propagated (37°C, 9.5% CO_2) in complete media: DMEM high glucose, 25 mM HEPES (Mediatech #15-018-CV), 10% Cosmic calf serum (HyClone #SH30087.03), penicillin and streptomycin, 2 mM glutamine, and 500 μg/ml active geneticin (G418). For transgene expression, tebufenozide (gift from Lynne Moore, Gage lab, Salk Institute) was added to the above media (200 nM final

concentration from 1 mM stock in 85% ethanol). Wildtype and Bax/Bak double-knockout MEF cells (generously provided by Craig B. Thompson, U. Penn) were grown in RPMI/ penicillin and streptomycin and 10% fetal bovine serum (Gibco #26140-079).

Cycloaddition reactions and in-gel fluorescence scanning

Cell lysates were prepared from 24-hour-induced Q103 cells by swelling (23×10^6 cells/ml in sodium phosphate buffer, pH 8.1, 5 min, 4°C), passing through a 30-gauge needle (10 strokes), and clarified (14,000 g, 20 min, 4°C). Clarified crude cell lysate (43 μl, 2×10^6 cell eq.) was incubated with alkyne-derivatized probe (16F16A or 16F16A-DC, 7 μmol, 1hr, RT) and Cu(I)-catalyzed Huisgen cycloaddition reactions (using RhN_3 or FcN_3 tags) were carried out as described[20]. Labeled lysates were prepared for SDS-PAGE analysis and visualized in-gel using Molecular Dynamics Fluorimager 595 and appropriate excitation and emission filters for the fluorphore. Competitive binding assays were performed as described above, except that cell lysates were pre-incubated for 1 hr at RT with 20× molar excess of the tested compound (competition controls were incubated with inactive analogs or equivalent addition of DMSO or water). Cystamine (C121509), hypotaurine (H1384) and bovine PDI (P3818) were purchased from Sigma-Aldrich.

Affinity purification and MS sequence identification

Uncoupled FcN_3 tag was removed from 16F16A-fluorescein-labeled lysates using Zebra desalting columns (Pierce #89882). Labeled proteins were affinity purified over anti-fluorescein-coupled affinity matrix (5 mg monoclonal anti-fluorescein coupled to NHS-activated sepharose, Amersham #17-0906-01) and eluted with 100 mM glycine (pH 2.8). Affinity purified proteins were analyzed by SDS-PAGE and fluorescently-tagged targets (major doublet at 53–57 kDa) were excised from the gel and submitted to Taplin Biological Mass Spectrometry Facility (Harvard Medical School) for protein identification. Tandem samples were run on SDS-PAGE and transferred to PVDF membranes for Western blot analysis using anti-PDI antibody.

Brain slice assays for HD and AD

Coronal brain slices (250 μm-thick) containing both cortex and striatum were prepared from CD Sprague-Dawley rat pups (Charles River) at postnatal day 10 using a Vibratome (Vibratome Co.). Brain slices were placed in 6-well plate transwell inserts (BD Biosciences) under which culture medium was added, containing 15% heat-inactivated horse serum, 10 mM KCl, 10 mM HEPES, 100 U/ml penicillin/streptomycin, 1 mM MEM sodium pyruvate, and 1 mM L-glutamine in Neurobasal A (Invitrogen). A biolistic device (Helios Gene Gun; Bio-Rad) was then used to transfect brain slices according to manufacturer's instructions; 1.6 μm gold particles were used with the device set at 95–105 psi and an aperture distance of ~2.5 cm. As the co-transfection linkage rate of biolistics approaches 100%, multiple DNAs can be reliably co-expressed in neurons by coating the gold particles with mixtures of independent expression plasmids. Thus, labeling of striatal or cortical neurons was done by mixing a separate plasmid driving YFP expression together with either an Htt or APP expression construct as described below, and a third plasmid expressing shRNA was added to the mixture for the RNAi knockdown studies. In all cases, total DNA load was balanced in control conditions where necessary by the addition of the corresponding empty vectors.

Compounds were added to the culture wells at the time of slice preparation and transfection, to a final DMSO concentration of 0.1%; the slices were then placed in humidified incubators under 5% CO2 at 32 deg. C.

For the HD brain slice model, YFP co-transfected medium spiny neurons (MSNs) were identified after 4 days of incubation by their location within the striatum and by their characteristic dendritic arborization using Leica MZFLIII fluorescent stereomicroscopes. MSNs exhibiting normal-sized cell bodies, even and continuous expression of YFP within all cell compartments, and >2 discernable primary dendrites > 2 cell bodies long were scored as “healthy”. The htt plasmid used to induce neurodegeneration of MSNs included human htt exon-1 containing a 73 polyglutamine repeat and was constructed based on clones and sequences that were generous gifts of Dr. Chris Ross (Johns Hopkins) and the Hereditary Disease Foundation. This htt sequence was cloned into the gWiz expression vector (Genlantis). Positive control KW+CGS was KW-6002 (50 μM) and CGS-21680 (30 μM); Boc-D-FMK (Sigma-Aldrich, Inc; 100μM).

For the AD brain slice model, cortical pyramidal neurons were assayed after 3 days of incubation and were readily discerned and unambiguously identified based on their characteristic positioning and orientation within the cortex, and by their striking morphological features, most notably the extension of a single, prominent apical dendrite radially towards the pial surface. These key features were used to determine the numbers of healthy cortical pyramidal neurons, namely 1) a robust and brightly labeled cell body positioned within the pyramidal neuronal layers of the cortex; 2) the retention of a clear apical dendrite extending radially towards the pial surface the slice; 3) the extension directly from the cell soma of >2 clear basal dendrites >2 cell body diameters long; and 4) clear and continuous cytoplasmic labeling with the YFP visual marker in the cell soma as well in all dendrites and the axon. In this brain slice assay, transfection of the normal human neural APP sequence (695 aa form) produces sufficient Aβ to induce neurodegeneration of cortical neurons, and this neurodegeneration could be blocked be either β- or γ-secretase inhibitors (Braithewaite et al., submitted). As above, this APP sequence was cloned into the gWiz expression vector.

Statistics

Primary screening parameters were adjusted (e.g., cell density and incubation time) to yield the best Z′ calculation between induced Q103 and Boc-D-FMK rescued cells. Mean and standard deviations for viability assays (run as biological triplicates) were plotted using Cricket Graph (interpolation function). For the *In vitro* PDI assay and drug/serum withdrawal apoptosis assay, non-linear regression was used to fit curves to the mean and standard deviations (N=3) calculated with GraphPad Prism™ software. For Western blot quantification, one representative sample of three or more experiments is shown. Statistical significance of shRNA rescue in PC12 cells was determined by ANOVA and Dunnett’s *post hoc* comparison test at the 0.01 confidence level. For the cortical-striatal brain slice assay, averages and SEM were calculated by counting 100 YFP positive MSNs from 20–22 slice assays. Statistical significance was determined by ANOVA and Dunnett’s post hoc comparison test at the 0.05 confidence level.

Supplementary Material

Refer to Web version on PubMed Central for supplementary material.

Acknowledgments

We thank E. Schweitzer for the transfected PC12 cell lines, C. Ross for Htt DNAs upon which the constructs used here were based, I. Smukste for assistance with organic synthesis, A. Bauer for assembling the BBB library, D. Dunn for additional brain slice experiments, and C. Thompson for the Bax/Bak double-knockout MEF cells. We are grateful to A. Speers, J. Alexander, and B. Cravatt for reagents and advice on the cycloaddition reactions; E. Miller, E. Signer, A. Tobin, N. Wexler, C. Johnson, R. Pacifici, and M. Finn for useful discussions; E. Miller and S. Hoffschmidt for editorial comments on the manuscript. This research was supported by grants from the NIH (NIGMS 1RO1GM085081; B.R.S. and NINDS R21NS048181; D.C.L.), the Hereditary Disease Foundation (D.C.L., B.R.S.), the High Q Foundation (B.R.S.), CHDI Foundation, Inc. (D.C.L., B.R.S.), the Arnold and Mabel Beckman Foundation (B.R.S.), the Training Program in Molecular Biophysics T32GM008281 (A.K), and a Burroughs Wellcome Fund Career Award at the Scientific Interface (B.R.S.). B.G.H. was supported in part by postdoctoral fellowship from the High Q Foundation. Brent R. Stockwell is an Early Career Scientist of the Howard Hughes Medical Institute.

References

1. Gregersen N. Protein misfolding disorders: pathogenesis and intervention. J Inherit Metab Dis. 2006; 29:456–70. [PubMed: 16763918]
2. Orr HT, Zoghbi HY. Trinucleotide repeat disorders. Annu Rev Neurosci. 2007; 30:575–621. [PubMed: 17417937]
3. Hickey MA, Chesselet MF. Apoptosis in Huntington's disease. Prog Neuropsychopharmacol Biol Psychiatry. 2003; 27:255–65. [PubMed: 12657365]
4. Thomas LB, et al. DNA end labeling (TUNEL) in Huntington's disease and other neuropathological conditions. Exp Neurol. 1995; 133:265–72. [PubMed: 7649231]
5. Reddy PH, et al. Behavioural abnormalities and selective neuronal loss in HD transgenic mice expressing mutated full-length HD cDNA. Nat Genet. 1998; 20:198–202. [PubMed: 9771716]
6. Hodgson JG, et al. A YAC mouse model for Huntington's disease with full-length mutant huntingtin, cytoplasmic toxicity, and selective striatal neurodegeneration. Neuron. 1999; 23:181–92. [PubMed: 10402204]
7. Kiechle T, et al. Cytochrome C and caspase-9 expression in Huntington's disease. Neuromolecular Med. 2002; 1:183–95. [PubMed: 12095160]
8. Yu ZX, et al. Mutant huntingtin causes context-dependent neurodegeneration in mice with Huntington's disease. J Neurosci. 2003; 23:2193–202. [PubMed: 12657678]
9. Ciammola A, et al. Increased apoptosis, Huntingtin inclusions and altered differentiation in muscle cell cultures from Huntington's disease subjects. Cell Death Differ. 2006; 13:2068–78. [PubMed: 16729030]
10. Bredesen DE, Rao RV, Mehlen P. Cell death in the nervous system. Nature. 2006; 443:796–802. [PubMed: 17051206]
11. Chipuk JE, Green DR. How do BCL-2 proteins induce mitochondrial outer membrane permeabilization? Trends Cell Biol. 2008; 18:157–64. [PubMed: 18314333]
12. Leber B, Lin J, Andrews DW. Embedded together: the life and death consequences of interaction of the Bcl-2 family with membranes. Apoptosis. 2007; 12:897–911. [PubMed: 17453159]
13. Jiang X, Wang X. Cytochrome C-mediated apoptosis. Annu Rev Biochem. 2004; 73:87–106. [PubMed: 15189137]
14. Chipuk JE, Bouchier-Hayes L, Green DR. Mitochondrial outer membrane permeabilization during apoptosis: the innocent bystander scenario. Cell Death Differ. 2006; 13:1396–402. [PubMed: 16710362]
15. Aiken CT, Tobin AJ, Schweitzer ES. A cell-based screen for drugs to treat Huntington's disease. Neurobiol Dis. 2004; 16:546–55. [PubMed: 15262266]

16. Huisgen, R. 1,3-Dipolar Cycloaddition Chemistry. Padwa, A., editor. Wiley; New York: 1984. p. 1-176.
17. Rostovtsev VV, Green LG, Fokin VV, Sharpless KB. A stepwise huisgen cycloaddition process: copper(I)-catalyzed regioselective “ligation” of azides and terminal alkynes. Angew Chem Int Ed Engl. 2002; 41:2596–9. [PubMed: 12203546]
18. Tornoe CW, Christensen C, Meldal M. Peptidotriazoles on solid phase: [1,2,3]-triazoles by regiospecific copper(i)-catalyzed 1,3-dipolar cycloadditions of terminal alkynes to azides. J Org Chem. 2002; 67:3057–64. [PubMed: 11975567]
19. Wang Q, et al. Bioconjugation by copper(I)-catalyzed azide-alkyne [3 + 2] cycloaddition. J Am Chem Soc. 2003; 125:3192–3. [PubMed: 12630856]
20. Speers AE, Cravatt BF. Profiling enzyme activities in vivo using click chemistry methods. Chem Biol. 2004; 11:535–46. [PubMed: 15123248]
21. Karpuj MV, et al. Prolonged survival and decreased abnormal movements in transgenic model of Huntington disease, with administration of the transglutaminase inhibitor cystamine. Nat Med. 2002; 8:143–9. [PubMed: 11821898]
22. Dedeoglu A, et al. Therapeutic effects of cystamine in a murine model of Huntington’s disease. J Neurosci. 2002; 22:8942–50. [PubMed: 12388601]
23. Van Raamsdonk JM, et al. Cystamine treatment is neuroprotective in the YAC128 mouse model of Huntington disease. J Neurochem. 2005; 95:210–20. [PubMed: 16181425]
24. Tremblay ME, et al. Neuroprotective effects of cystamine in aged parkinsonian mice. Neurobiol Aging. 2006; 27:862–70. [PubMed: 15913845]
25. Wilkinson B, Gilbert HF. Protein disulfide isomerase. Biochim Biophys Acta. 2004; 1699:35–44. [PubMed: 15158710]
26. Ellgaard L, Ruddock LW. The human protein disulphide isomerase family: substrate interactions and functional properties. EMBO Rep. 2005; 6:28–32. [PubMed: 15643448]
27. Rigobello MP, Donella-Deana A, Cesaro L, Bindoli A. Distribution of protein disulphide isomerase in rat liver mitochondria. Biochem J. 2001; 356:567–70. [PubMed: 11368786]
28. Turano C, Coppari S, Altieri F, Ferraro A. Proteins of the PDI family: unpredicted non-ER locations and functions. J Cell Physiol. 2002; 193:154–63. [PubMed: 12384992]
29. Vance JE. Phospholipid synthesis in a membrane fraction associated with mitochondria. J Biol Chem. 1990; 265:7248–56. [PubMed: 2332429]
30. Rizzuto R, et al. Close contacts with the endoplasmic reticulum as determinants of mitochondrial Ca2+ responses. Science. 1998; 280:1763–6. [PubMed: 9624056]
31. Hayashi T, Su TP. Sigma-1 receptor chaperones at the ER-mitochondrion interface regulate Ca(2+) signaling and cell survival. Cell. 2007; 131:596–610. [PubMed: 17981125]
32. Hayashi T, Rizzuto R, Hajnoczky G, Su TP. MAM: more than just a housekeeper. Trends Cell Biol. 2009
33. Lindsten T, et al. The combined functions of proapoptotic Bcl-2 family members bak and bax are essential for normal development of multiple tissues. Mol Cell. 2000; 6:1389–99. [PubMed: 11163212]
34. Nie C, et al. Cysteine 62 of Bax is critical for its conformational activation and its proapoptotic activity in response to H2O2-induced apoptosis. J Biol Chem. 2008; 283:15359–69. [PubMed: 18344566]
35. Khoshnan A, et al. Activation of the IkappaB kinase complex and nuclear factor-kappaB contributes to mutant huntingtin neurotoxicity. J Neurosci. 2004; 24:7999–8008. [PubMed: 15371500]
36. Varma H, Cheng R, Voisine C, Hart AC, Stockwell BR. Inhibitors of metabolism rescue cell death in Huntington’s disease models. Proc Natl Acad Sci U S A. 2007; 104:14525–30. [PubMed: 17726098]
37. Southwell AL, et al. Intrabodies binding the proline-rich domains of mutant huntingtin increase its turnover and reduce neurotoxicity. J Neurosci. 2008; 28:9013–20. [PubMed: 18768695]
38. Thinakaran G, Koo EH. Amyloid precursor protein trafficking, processing, and function. J Biol Chem. 2008; 283:29615–9. [PubMed: 18650430]

39. Braithwaite SP, et al. Inhibition of c-Jun kinase provides neuroprotection in a model of Alzheimer's disease. Neurobiol Dis. 2010; 39:311–17. [PubMed: 20451607]
40. Friedlander RM, Brown RH, Gagliardini V, Wang J, Yuan J. Inhibition of ICE slows ALS in mice. Nature. 1997; 388:31. [PubMed: 9214497]
41. Ona VO, et al. Inhibition of caspase-1 slows disease progression in a mouse model of Huntington's disease. Nature. 1999; 399:263–7. [PubMed: 10353249]
42. Chen M, et al. Minocycline inhibits caspase-1 and caspase-3 expression and delays mortality in a transgenic mouse model of Huntington disease. Nat Med. 2000; 6:797–801. [PubMed: 10888929]
43. Zhu S, et al. Minocycline inhibits cytochrome c release and delays progression of amyotrophic lateral sclerosis in mice. Nature. 2002; 417:74–8. [PubMed: 11986668]
44. Graham RK, et al. Cleavage at the caspase-6 site is required for neuronal dysfunction and degeneration due to mutant huntingtin. Cell. 2006; 125:1179–91. [PubMed: 16777606]
45. Galvan V, et al. Reversal of Alzheimer's-like pathology and behavior in human APP transgenic mice by mutation of Asp664. Proc Natl Acad Sci U S A. 2006; 103:7130–5. [PubMed: 16641106]
46. Atkin JD, et al. Induction of the Unfolded Protein Response in Familial Amyotrophic Lateral Sclerosis and Association of Protein-disulfide Isomerase with Superoxide Dismutase 1. J Biol Chem. 2006; 281:30152–65. [PubMed: 16847061]
47. Conn KJ, et al. Identification of the protein disulfide isomerase family member PDIp in experimental Parkinson's disease and Lewy body pathology. Brain Res. 2004; 1022:164–72. [PubMed: 15353226]
48. Yoo BC, et al. Overexpressed protein disulfide isomerase in brains of patients with sporadic Creutzfeldt-Jakob disease. Neurosci Lett. 2002; 334:196–200. [PubMed: 12453628]
49. Uehara T, et al. S-nitrosylated protein-disulphide isomerase links protein misfolding to neurodegeneration. Nature. 2006; 441:513–7. [PubMed: 16724068]
50. Bailey CD, Johnson GV. The protective effects of cystamine in the R6/2 Huntington's disease mouse involve mechanisms other than the inhibition of tissue transglutaminase. Neurobiol Aging. 2006; 27:871–9. [PubMed: 15896882]

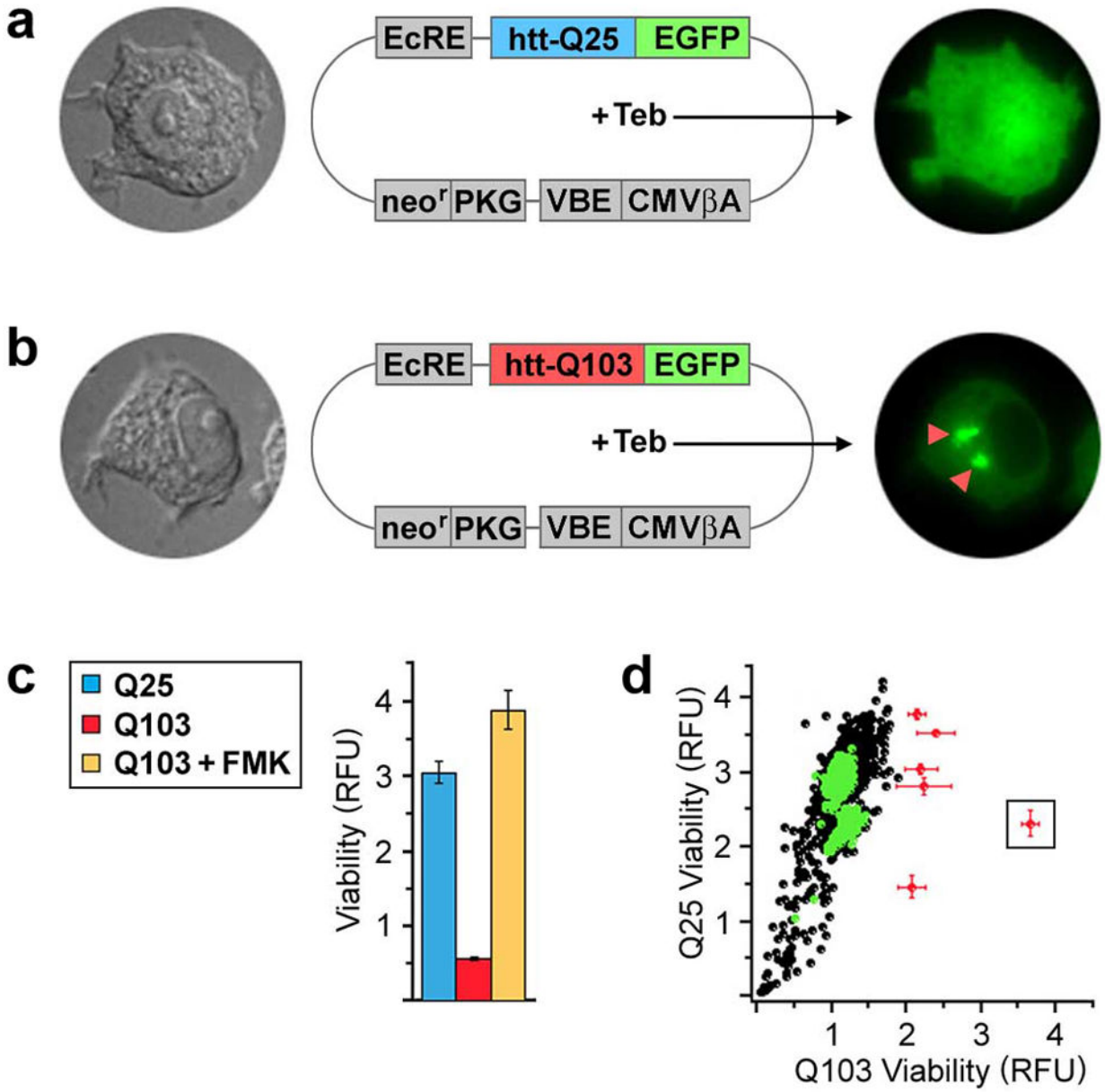

Figure 1. Cell-based (PC12) model of mutant huntingtin protein misfolding and cell toxicity

(**a**) Cells transfected with an inducible plasmid containing wild-type huntingtin (htt-Q25) show diffuse protein expression throughout the cytosol (24 hrs post-induction with the ecdysone analog tebufenozide, Teb). (**b**) Cells transfected with the same plasmid containing mutant, polyQ-expanded huntingtin (htt-Q103), show perinuclear inclusion bodies at 24 hrs post-induction (red arrowheads). (**c**) Cell viability of mutant-huntingtin-expressing cells is decreased to less than 20% of the wild-type expressing cells (measured by Alamar Blue fluorescence at 48 hrs post-induction). Cell death induced by htt-Q103 can be rescued by treatment with a general caspase inhibitor, Boc-D-FMK (FMK, 50 μM). (**d**) Primary screening results of 2,036 compounds showing effects on cell viability of induced Q25 and Q103 cells. Putative hit compounds that rescue Q103-induced cell death are shown in red,

confirmed hit (thiomuscimol) is boxed, DMSO treated controls shown in green. Plasmid abbreviations: ecdysone responsive element (EcRE), wild-type huntingtin exon-1 (htt-Q25), mutant huntingtin exon-1 (htt-Q103), enhanced green fluorescent protein (EGFP), VP16-ecdysone receptor chimera (VBE), cytomegalovirus enhancer/beta-actin promoter (CMV-bA), neomycin resistance (PKG-neo^r).

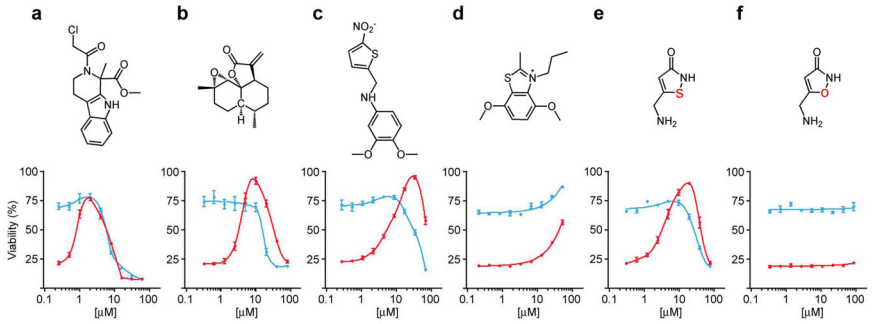

Figure 2. Dose-response curves for hit compounds that suppress Q103-induced apoptosis

The viability of tebufenozide-induced htt-Q25 (blue) and htt-Q103 (red) cells was detected by Alamar Blue fluorescence and plotted as a percentage of uninduced cells at 48 hours post-induction. (**a**) 16F16, (**b**) arteannuin B, (**c**) BBC7M13, (**d**) BBC7E8, (**e**) thiomuscimol, (**f**) muscimol (inactive analog of thiomuscimol; single atom substitution shown in red).

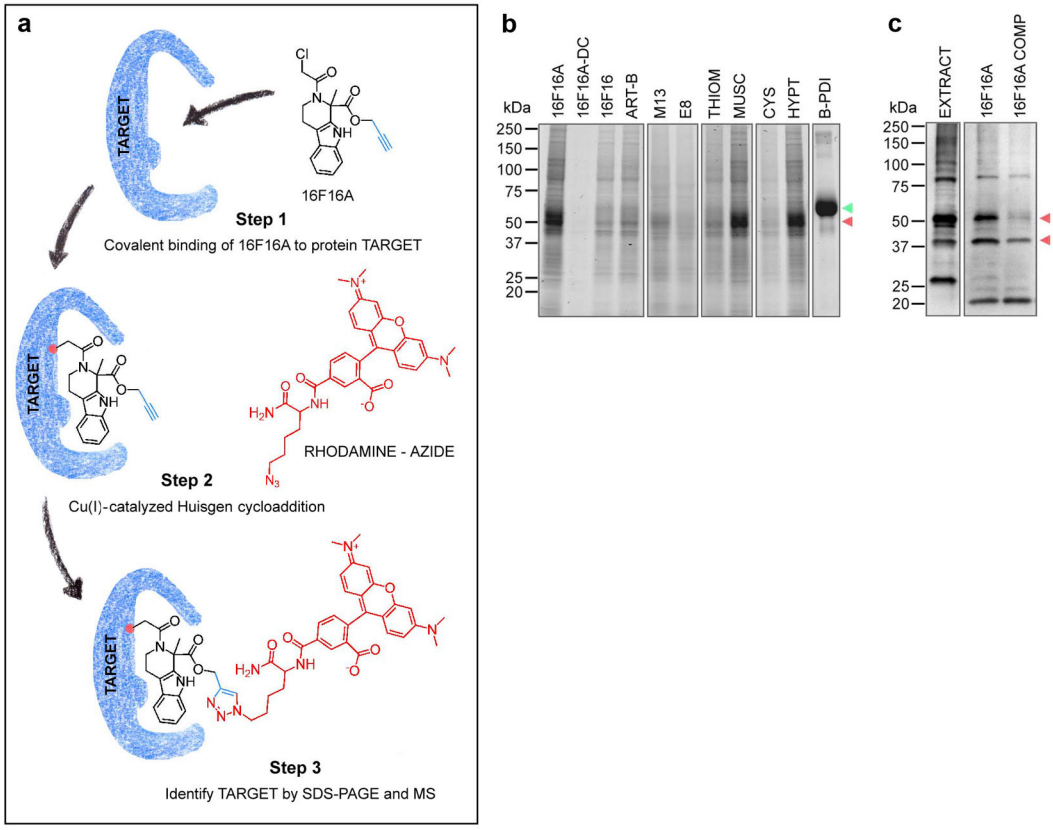

Figure 3. Identification of small molecule target proteins using Huisgen cycloaddition chemistry

(**a**) Fluorescent tagging of small molecule target proteins. Step 1: alkyne derivatized-16F16 (16F16A) covalently binds to target proteins in PC12 lysate. Step 2: alkyne derivatized-16F16 (16F16A) is coupled to rhodamine-azide via Cu(I)-catalyzed Huisgen 1,3-dipolar cycloaddition reaction. Step 3: fluorescently-tagged target proteins are affinity purified, analyzed by SDS-PAGE, and identified as by mass spectrometry (MS) as rat protein disulfide-isomerase precursors (PDIA1 and PDIA3). (**b**) Laser scanned gel of 16F16A-rhodamine tagged proteins (PDI = 53 kDa doublet, red arrowhead) in crude PC12 extract (16F16A-DC = inactive deschloro-16F16 propargyl analog, structure Fig. 4a). Pretreatment of PC12 extract with 16F16, arteannuin B (ART-B), BBC7M13 (M13), BBC7E8 (E8), thiomuscimol, or cystamine blocks 16F16A target binding. Inactive analogs muscimol and hypotaurine do not compete for 16F16A target binding. Purified bovine PDI (B-PDI) is covalently labeled by 16F16A-rhodamine (green arrowhead). (**c**) Anti-PDI Western blot of affinity purified 16F16A target proteins confirms the sequence data (full length 53 kDa and 38 kDa proteolytic PDI fragment; red arrowheads). Extract = crude PC12 extract, 16F16A = affinity-purified 16F16A, fluorescein-tagged target from PC12 extract, 16F16A comp = pre-treatment of PC12 extract with 20× 16F16, followed by addition of 16F16A, fluorescein-azide coupling, and affinity purification.

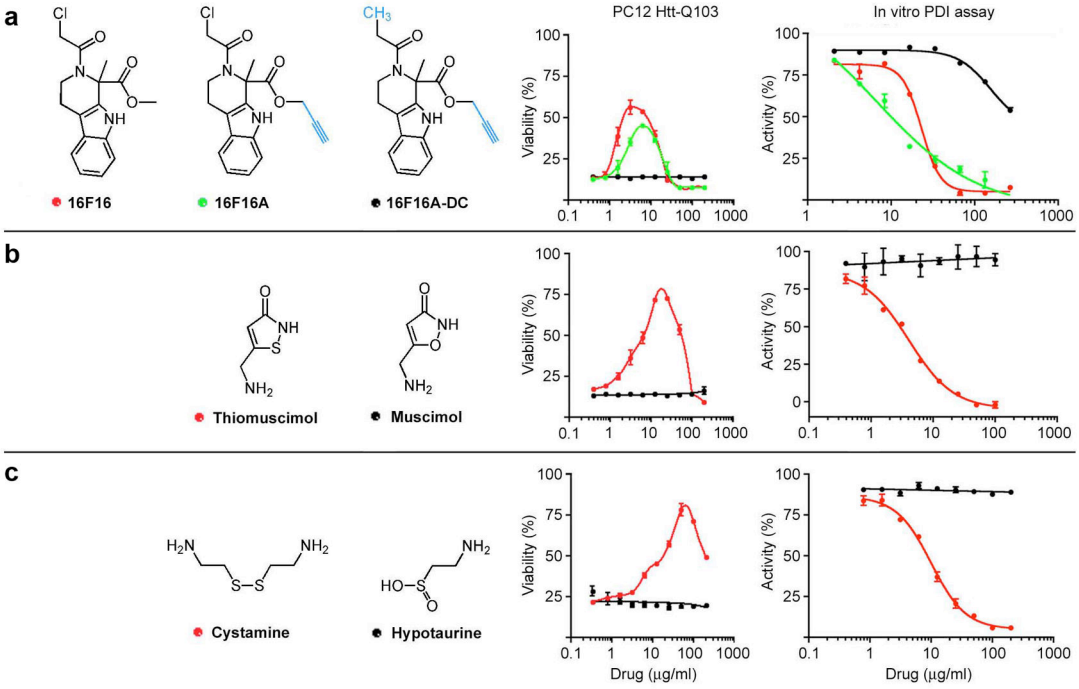

Figure 4. Compounds that bind to PDI and rescue htt-Q103-induced toxicity inhibit PDI reductase activity *in vitro*

(**a**) 16F16 and 16F16 propargyl analogs (structural modifications shown in blue), (**b**) thiomuscimol and its inactive analog muscimol, (**c**) cystamine and an inactive analog hypotaurine.

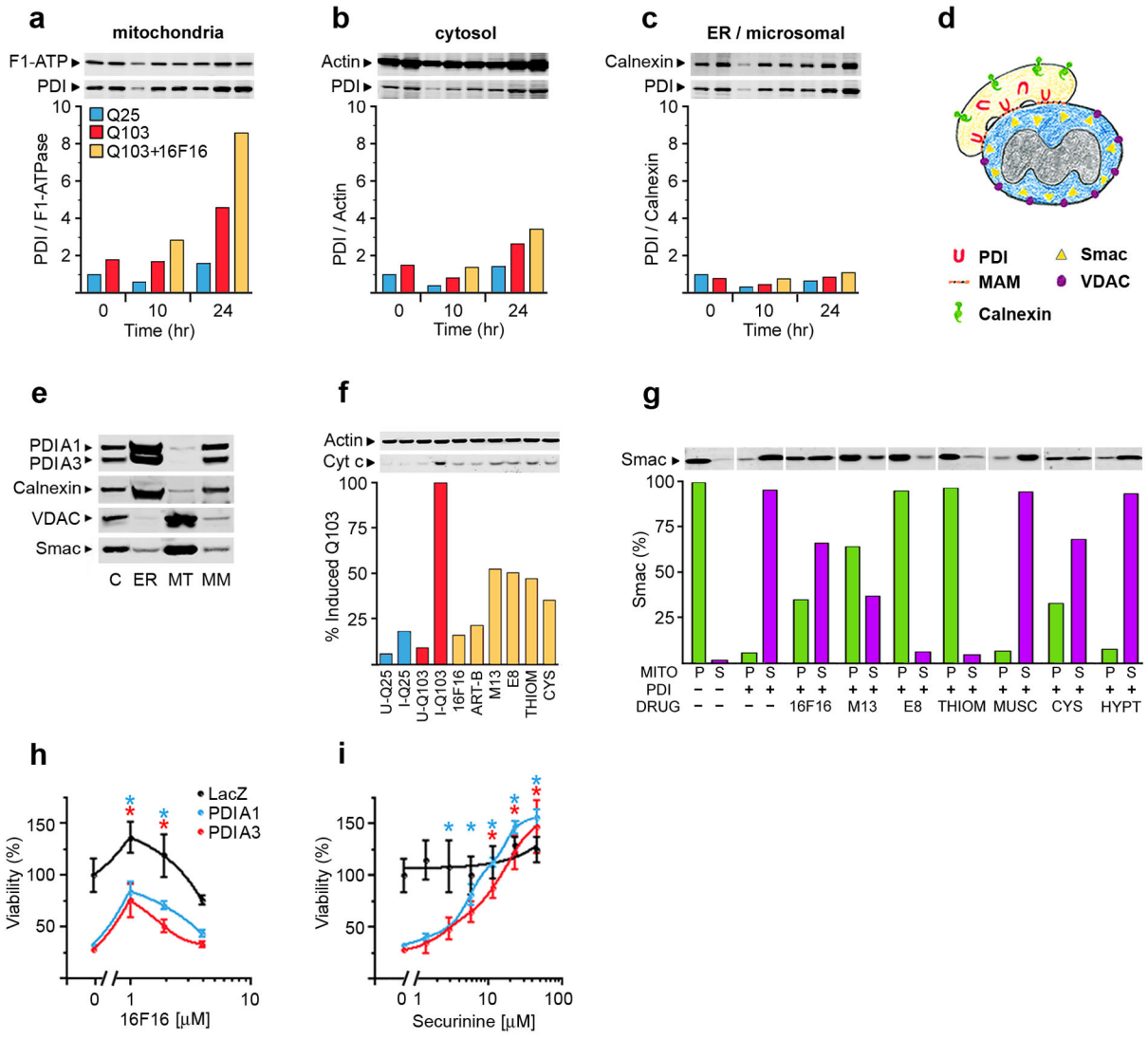

Figure 5. PDI accumulates at MAM contacts and induces MOMP

(**a–c**) Western blot and LI-COR quantification of PDIA1 in mitochondrial, cytosolic, and ER/microsomal cell fractions (nomalized to F_1-ATPase, actin, and calnexin respectively). Time-course analysis shows a 2.8-fold increase of Q103 mitochondrial PDI over Q25 mitochondrial PDI at 24 hrs post-induction. Induced Q103 cells rescued with 16F16 (7.8 μM) show a 5.3 fold increase of mitochondrial PDI over induced Q25 cells at 24 hrs. (**d**) Drawing of the MAM architecture. (**e**) Western blot analysis of purified mitochondrial and associated membrane (MAM) fractions. Crude (sucrose gradient purified) mitochondria isolated from Q103-expressing cells (Lane C) were further purified by Percoll gradient centrifugation to isolate the MAM fraction[29]. The MAM fraction is shown to contain PDIA1 and PDIA3 protein. Abbreviations: crude mitochondria (C), microsomal/ER fraction (ER), purified mitochondrial fraction (MT), MAM fraction (MM). (**f**) LI-COR quantification of cytosolic cytochrome c in Q25 and Q103-expressing cells. (**g**) Mitochondrial MOMP assay using purified PC12 mitochondria. The mitochondria were then pelleted and the degree of MOMP calculated as a percentage of Smac released from the mitochondrial pellet (P) into

the supernatant (S). PDI inhibitors 16F16, BBC7M13 (M13), BBC7E8 (E8), thiomuscimol (THIOM), and cystamine (CYS) suppress PDI-driven MOMP, whereas inactive analogs muscimol (MUSC) and hypotaurine (HYPT) do not suppress Smac release. Abbreviations: uninduced (U), induced (I). (**h–i**) Overexpressing PDIA1 or PDI-3 in PC12 cells induces apoptosis that is suppressed by PDI inhibitors (rescue over untreated cells calculated by ANOVA and Dunnett's *post hoc* comparison test at the 0.01 confidence level). Supplementary Fig. 8 shows the characterization of securinine, which we identified as an additional PDI inhibitor.

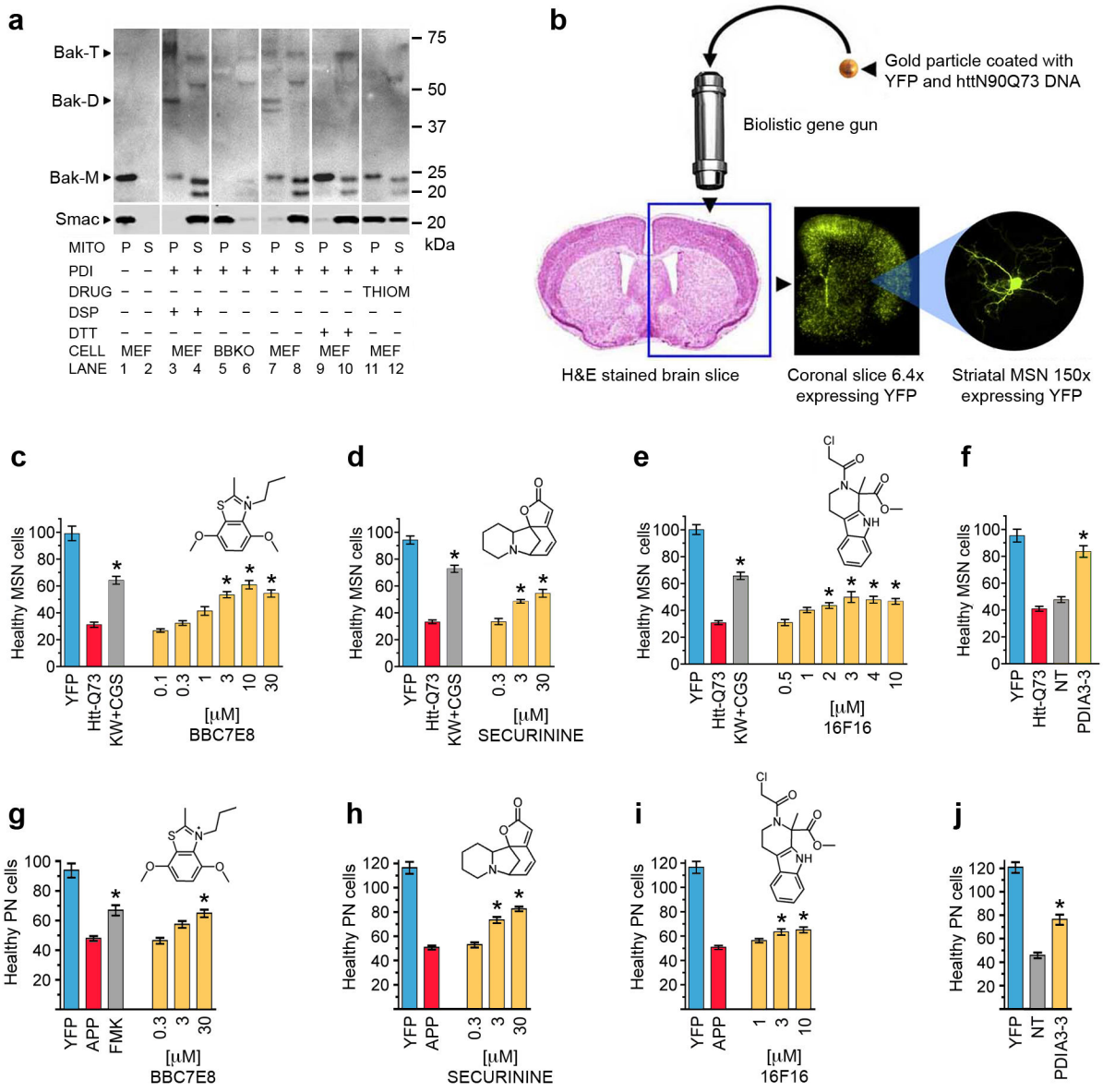

Figure 6. Characterization of PDI-induced MOMP and validation in model systems

(**a**) Mitochondrial MOMP assay using mouse embryonic fibroblast (MEF) and Bax/Bak double knockout (BBKO) MEF cells. Western blot analysis for Smac and Bak protein demonstrates that PDI-induced MOMP takes place in the absence of cytosol and is mediated by oligomerization of mitochondrial Bak (lanes 1–6; Bak-M, D, and T correspond to Bak monomer, dimer, and trimer respectively). The Bak protein is oligomerized via oxidation of cystein residues (lanes 7–10). Oligomerization of Bak and mitochondrial release of Smac is suppressed by inhibiting PDI with thiomuscimol (THIOM; lanes 11 and 12). DSP= Dithiobis (succinimidyl) propionate; homobifunctional and membrane permeable crosslinker. (**b**) Schematic diagram of the rat corticostriatal brain slice assay (data in **c–j**). (**c–e**) Small molecule PDI inhibitors suppress htt-N90Q73-induced toxicity in brain slice MSNs (**c**) BBC7E8, (**d**) securinine, and (**e**) 16F16. (**f**) Knockdown of PDIA3 using a

validated A3-3 shRNA targeting plasmid (Supplementary Fig. 6) suppresses htt-N90Q73 toxicity in brain slice MSNs. (**g–i**) PDI inhibitors and shRNA suppress APP/Aβ toxicity in brain slice pyramidal neurons (**g**) BBC7E8, (**h**) securinine, (**i**) 16F16, (**j**) PDIA3 shRNA. Controls and legend: YFP (transfection control), KW+CGS (chemical rescue of htt-N90Q73 by KW-6002 and CGS21680), NT (non-targeting shRNA), FMK (caspase inhibitor Boc-D-FMK, 100μM), PN (pyramidal neurons); yellow bars are inhibitor treated (PDI inhibitor or shRNA) htt-N90Q73 or APP/Aβ expressing cells; asterisks represent a statistically significant (ANOVA and Dunnett's *post hoc* comparison test at the 0.05 confidence level) rescue of htt-Q73 or APP/Aβ toxicity.